Research paper

Pulmonary delivered polymeric micelles – Pharmacokinetic evaluation and biodistribution studies

CrossMark

Xiao Hu [a], Fei-Fei Yang [a], Li-Hui Quan [a], Chun-Yu Liu [a], Xin-Min Liu [a], Carsten Ehrhardt [b], Yong-Hong Liao [a,*]

[a] Institute of Medicinal Plant Development, Chinese Academy of Medical Sciences & Peking Union Medical College, Beijing, China
[b] School of Pharmacy and Pharmaceutical Sciences, Trinity College Dublin, Dublin, Ireland

ARTICLE INFO

ABSTRACT

Polymeric micelles represent interesting delivery systems for pulmonary sustained release. However, little is known about their *in vivo* release and translocation profile after delivery to the lungs. In the present study, curcumin acetate (CA), which is an ester prodrug of curcumin, or the mixture of CA and Nile red was encapsulated into PEG–PLGA micelles by a solvent evaporation method. The micellar formulation increased the stability of CA in water and physiologically relevant fluids and led to a sustained drug release *in vitro*. Following intratracheal (IT) administration to rats, CA loaded micelles achieved not only prolonged pulmonary retention with AUC values almost 400-fold higher than by IV route, but also local sustained release up to 24 h. In addition, IT delivery of micelles appeared to facilitate the uptake into the pulmonary vascular endothelium and efficiently translocate across the air–blood barrier and penetrate into the brain. Co-localization of CA and Nile red confirmed that micelles in lung and brain tissue were still intact. This study is the first to demonstrate that aerosolized PEG–PLGA micelles are a promising carrier for both pulmonary and non-invasive systemic sustained release of labile drugs.

© 2014 Elsevier B.V. All rights reserved.

1. Introduction

Curcumin is the major active ingredient of *Curcuma longa* rhizome (popularly known as turmeric). The compound has been associated with anti-oxidant, anti-inflammatory and immunomodulatory pharmacological effects [1]. As an NF-κB inhibitor, curcumin has exhibited protective effects in chronic hypoxic hypercapnic and monocrotaline (MCT) induced pulmonary arterial hypertension (PAH) in rats [2,3] and it is thus considered as a potential therapeutic agent for PAH [4].

PAH is a chronic and intractable disease characterized by an elevation in pulmonary artery pressure that leads to right-sided heart failure and premature death [5]. Various pharmacological treatments, including prostacyclin analogues such as epoprostenol, treprostinil and iloprost, endothelin receptor antagonist such as bosentan, and phosphodiesterase 5 inhibitors such as sildenafil and tadalafil, have been approved for this life-threatening disorder, and these interventions can improve symptoms and quality of life for moderate and severe PAH [5–8]. However, most drugs have a very short half-life, often requiring continuous subcutaneous or intravenous infusion to elicit their therapeutic benefit. Meanwhile, systemic exposure of anti-PAH agents can induce off-target actions and result in minor or sometimes even severe side effects, leading to limited treatment compliance [9]. Consequently, non-invasive delivery of inhaled prostacyclins is considered as the most promising means to minimize the systemic side effects while achieving effective pulmonary vasodilation [9,10]. Yet, the existing inhaled medications require repeated dosing (e.g., 6–9 times for inhaled iloprost) due to rapid pulmonary clearance and commonly lead to cough and throat irritation [11–13]. These limitations of current inhaled therapy necessitate the development of novel inhalable formulations that can achieve pulmonary sustained release, or

ideally directly target the pulmonary arterial endothelial cells, and to avoid local irritation.

In this context, microparticles [14–17], liposomes [18–20], nanoparticles [21,22], PEG-lipid micelles [23] and nanocrystals [24] have been investigated, and some different nanocarriers have been used to achieve pulmonary sustained release [24–28].

Due to its poor physicochemical and biopharmaceutical properties including very labile stability, poor oral bioavailability and rapid systemic elimination, the clinical use of curcumin is limited. Systemic delivery of curcumin loaded nanoparticles tends to meet difficulty in achieving therapeutic level of the drug in the lung for anti-PAH since the thickened pulmonary vascular wall under PAH pathological condition restrains nanoparticles from extravasating through the vessels to the lung [29]. Considering the fact that polymeric micelles have the property to extend pulmonary drug release [30] and esterified prodrugs can prolong pulmonary retention [31], mPEG–PLGA micelles might be utilized as carriers for the encapsulation of CA, an acetate prodrug of curcumin.

The main objective of this study was to determine the *in vivo* release and translocation profiles of micelles after delivery to the lungs, which were largely uninvestigated in previous studies on inhaled micellar/liposomal systems. The further objective was to test the hypothesis that CA-loaded mPEG–PLGA micelles via the pulmonary route were effective carriers for providing sustained levels of curcumin in the lung and thus increase the local accumulation of the drug in the pulmonary arteries.

2. Materials and methods

2.1. Materials

CA and curcumin with a purity >98% (determined by HPLC and differential scanning calorimetry, DSC) were donated by Ding-Guo Biotechnology Co., Ltd., (Beijing, China). Leucine was purchased from Alfa Aesar (Ward Hill, MA, USA). Nile red and coumarin-6 were purchased from Sigma–Aldrich (St. Louis, MO, USA). Aloe-emodin was obtained from the National Institute for the Control of Pharmaceutical and Biological Products (Beijing, China). $MPEG_{2000}$-$PLGA_{5000}$ (LA:GA = 75:25) was purchased from Shandong Dai Gang Biotechnology Co., Ltd (Shandong, China). Acetonitrile (ACN) and tetrahydrofuran (THF) of HPLC grade were obtained from Merck (Darmstadt, Germany) and formic acid of HPLC grade from Dima (Lake Forest, CA, USA). Water was purified by a Milli-Q water purification system (Millipore, Bedford, MA, USA). All other chemicals and reagents were of analytical grade.

2.2. Preparation and characterization of CA-loaded mPEG–PLGA micelles

2.2.1. Preparation

Micelles loaded either with CA or a mixture of CA and Nile red or coumarin-6 (5:1) were prepared according to the previously published solvent evaporation method [32]. Briefly, CA, Nile red/coumarin-6 and $mPEG_{2000}$-$PLGA_{5000}$ (1:40, w/w) were co-dissolved in dichloromethane. The organic solvent was evaporated under vacuum to form a film, followed by the addition of pre-warmed water in the presence of leucine (1% of the polymer) at 50 °C. Finally, the non-incorporated drug was removed by filtering through a 220 nm nylon membrane and the filtrates were subjected to characterization and freeze-drying.

2.2.2. Dynamic light scattering

Before measurements, the micellar dispersions without freeze-drying or the reconstituted dispersions after freeze-drying were subjected to 200-fold dilution. The hydrodynamic diameter of the micelles was measured by dynamic light scattering using a Zetasizer Nano ZS (Malvern Instruments Ltd., Malvern, UK) equipped with a 10 mW HeNe laser at a wavelength of 633 nm an a temperature of 25 °C. Scattered light was detected at 173° angle with laser attenuation and measurement position adjusted automatically by the instrument's software. The particle size was calculated automatically based on the scattered light and the Brownian motion of the particles using the Stokes–Einstein equation

$$Rh = kBT/6\pi\eta D$$

With the radius of the particles being *Rh*, the Boltzmann constant is *kB*, the absolute temperature *T*, the solvent viscosity η, and the diffusion coefficient *D*. Values given are the means ± SD of three different experiments with each experiment comprising three measurements of the same sample with at least 10 runs, as determined by the Zetasizer.

2.2.3. Laser Doppler velocimetry

The zeta-potential was measured with a Zetasizer Nano ZS at 25 °C and a scattering angle of 17° by measuring the electrophoretic mobility with laser Doppler velocimetry. Values given are the means ± SD of three different experiments with each experiment comprising three measurements of the same sample with at least 10 runs, as determined by the Zetasizer.

2.2.4. In vitro release

The *in vitro* release was performed in a dialysis bag (Spectra/Por® molecular weight cut off (MWCO) 8,000–14,000 Da, Spectrum Laboratories, Rancho Dominguez, CA, USA) against water containing 2% sodium dodecyl sulfate (SDS) under continuous 800 rpm magnetic stirring at 37 °C. The presence of SDS could improve the stability of released CA. The amount of CA in the receiving phase was determined by an HPLC assay as described in Section 2.5.1 and the fluorescence activity of Nile red and coumarin-6 was analyzed using a fluorescence microplate reader (Fluoroskan Ascent FL, Thermo Fisher Scientific, Waltham, MA, USA) at excitation and emission wavelengths of 530 nm and 590 nm (Nile red) and 430 nm and 538 nm (coumarin-6), respectively. All experiments were carried out in triplicate.

2.2.5. Encapsulation efficiency

The CA or Nile red/coumarin-6 loading content (DL) and encapsulation efficiency (EE) were determined as reported previously [32].

2.3. Stability of CA in micelles

CA solution in ACN and micellar dispersions were evaluated for stability in water or PBS buffer (pH 7.4) at a final concentration of 100 μg/ml and incubated at 40 °C with continuous magnetic stirring protected from light. The temperature of 40 °C was selected due to the fact that at this temperature, the stability could be differentiated between free drug and encapsulated drug in water or PBS buffer. At predetermined time intervals, samples of 200 μl were withdrawn for HPLC assay (see below).

The stability of CA solution and micellar dispersions in rat plasma at the concentration of 100 μg/ml was performed by incubation in an ice-water bath. At predetermined time intervals, samples of 100 μl were withdrawn and 200 μl ACN with aloe-emodin (internal standard) was added to quench esterase activity. The analytes were vortexed and centrifuged, and the supernatant was injected to HPLC (see below).

2.4. Pharmacokinetics and tissue distribution

2.4.1. Animals

Male Wistar rats (180–220 g, 8 weeks) were supplied by Institute of Laboratory Animal Science, Chinese Academy of Medical Sciences (Beijing, China). Prior to the experiments, all rats were housed at specific pathogen free animal rooms at temperature-controlled (22 ± 2 °C) and under 12 h light/dark cycles for at least 7 days, and the rats had free access to diet and water. On the day before the pharmacokinetic experiment, a polyethylene catheter (Portex Limited, Hythe, Kent, UK) was catheterized into the right jugular veins of the rats under pentobarbital sodium anesthesia (40 mg/kg). All animal experiments were performed under the instruction of regulations by the Animal Care and Use Committee of the Chinese Academy of Medical Sciences.

2.4.2. Pharmacokinetic study

CA was dissolved in an aqueous solution containing 25% (v/v) propanediol and 25% (v/v) hydrogenated castor oil for the free drug solution, whereas the freeze-dried CA-mPEG–PLGA powders were dissolved in water. After recovery from surgery for at least 12 h, the intubated rats were randomly assigned into three groups and received either intravenous administration of free CA solution (IV free drug group), micellar dispersions (IV micelle group) or intratracheal (IT) administration of micellar dispersions (IT micelle group), respectively, at a dose of 2 mg/kg. For IT administration, animals were anesthetized by an intraperitoneal injection of pentobarbital sodium (40 mg/kg). Subsequently, a curved balled needle of the micro-sprayer (Model IA-1B, Penn-Century Inc., USA) attached on a syringe was inserted into the trachea under visual guidance, and the micellar dispersion was delivered at a volume of 1.0 ml/kg. After intratracheal dosing, the animals were held in an upright position for 1 min to ensure deposition of the dose following the removal of the delivery device.

After dosing, aliquots of 200 μl blood samples were taken at 5, 10, 15, 20, 30, 45 and 60 min for IV free drug group and 5, 15, 30, 45, 60 min, 2, 4, 6, 8, 10, 12 and 24 h in case of the IV and IT micelle groups. Subsequently, 100 μl of plasma was obtained by immediate centrifugation of the blood at 5000 rpm for 2 min at 0 °C, followed by the addition of 200 μl ACN to quench the esterase activity. Samples were stored at −20 °C until further analysis.

2.4.3. Tissue distribution studies

All rats were assigned into three groups and administered with formulations as described in the previous section either IV injection or IT administration. At predetermined time points (i.e., 0.5, 1, 2, 4, 8, 12, 24 h) after dosing, three rats at each time point were euthanized by cervical dislocation, and the heart, liver, spleen, lung, kidney, brain and axillary lymph nodes were collected, washed and weighed. After tissue collection, samples were stored at −20 °C until further analysis.

2.5. HPLC analysis of CA in plasma and tissues

2.5.1. Chromatographic conditions

The HPLC system consisted of a Waters 2695 Sysyem, a Waters 2487 dual channel UV detector set at a wavelength of 420 nm, Empower software (Milford, MA, USA), and a C-18 Phenomenex® column (250 mm × 4.6 mm, 5 μm, Phenomenex Inc., Torrance, CA, USA) connected to a Phenomenex guard column. A gradient mobile phase system consisting of ACN:THF:H_2O (0–2 min 35:45:20, 2–4 min 35:45:20 ∼ 45:10:45, 4–7 min 45:10:45, 7–8.6 min 45:10:45 ∼ 35:45:20, 8.6–12 min 35:45:20) with 0.1% formic acid as a modifier, was used for the analysis of CA and converted curcumin. The flow rate was set to 1.0 min/ml. The column

temperature was maintained at 30 °C, whereas the sample temperature was set to 4 °C.

Under these chromatographic conditions, the total run time was 20 min with the retention time of 8.5 min and 13.1 min for curcumin and CA, respectively. Standard curves were prepared in the ranges of 4–1000 ng/ml and 0.005–20 μg/g for curcumin, 8–2000 ng/ml and 0.01–40 μg/g for CA, respectively, in plasma and tissue homogenates (except for the brain). Standard curves in brain were 0.5–125 ng/g and 1.25–125 ng/g for curcumin and CA, respectively. The method validation included the determination of precision, accuracy and extraction recovery, where five quality control samples of different concentration were prepared separately. A signal-to-noise ratio (S/N) of 3 and 10 was determined as the lower limit of detection (LLOD) and the lower limit of quantification (LLOQ), respectively. The relative standard deviations (RSD) for the inter-day and intra-day method's precision were below 5.96% and 6.92%, indicating that the method had acceptable precision. The method's accuracy was well within the proposed limits with all obtained values between 90% and 110%. The method's extraction recovery also satisfied the proposed limits, with all obtained values being higher than 70%. The LLOQ of curcumin was determined to be 4 ng/ml and 5 ng/g in plasma and tissue (except for the brain) homogenates, while for CA in plasma and tissue (except for the brain) homogenates were 8 ng/ml and 10 ng/g, respectively. The LLOD was determined to be 2 ng/ml and 2 ng/g for curcumin in plasma and tissue (except for the brain) homogenates, while for CA in plasma and tissue (except for the brain) homogenates were 4 ng/ml and 4 ng/g, respectively. The LLOQ was determined to be 0.5 ng/g and 1.25 ng/g for curcumin and CA in brain. The LLOD was determined to be 0.2 ng/g and 0.5 ng/g for curcumin and CA in brain.

2.5.2. Extraction of CA from plasma and tissue homogenate samples

The extraction of CA from plasma was performed at 0 °C by adding 10 μl aloe-emodin solution, 100 μl 10% (w/v) SDS solution and 1 ml ethyl acetate. The mixture was vortex mixed for 60 s and centrifuged at 12,000 rpm for 3 min. Then the organic upper layers were transferred to a new tube and dried under a nitrogen stream at room temperature. The residue was reconstituted in 200 μl of 80% ACN and vortexed for 60 s. After another centrifugation step at 12,000 rpm for 3 min, the supernatant was injected onto the HPLC system.

Tissue samples were homogenized in saline in the ratio of 1:3 (wt/wt). Subsequently, 200 μl tissue homogenate (except for the brain) was transferred to a tube followed by adding 10 μl aloe-emodin solution, 100 μl 10% w/v SDS solution and 1 ml ethyl acetate to extract CA and curcumin. All brain homogenate were used for extraction. After vortexing and centrifugation at 12,000 rpm for 3 min, the organic phase of each tube was transferred to a new tube and evaporated to dryness under a nitrogen stream at room temperature. The residue was reconstituted in 200 μl of 80% ACN and vortexed for 60 s. After centrifugation at 12,000 rpm for 3 min, the supernatant was transferred to HPLC vials and then 50 μl was injected onto the HPLC system.

2.6. Confocal laser scanning microscopy

The distribution and localization of micelles encapsulating the mixture of CA and Nile red in lung and brain tissues was monitored by confocal laser scanning microscopy (Zeiss LSM710, Göttingen, Germany). Before initiation of the microscopic experiments, CA and Nile red loaded micelles were administered to the rats by either the IV or IT route, and three rats were sacrificed and cardiac perfused at each predetermined time point (i.e., 1, 4 and 24 h) after dosing. Subsequently, the lung and brain tissues were removed, washed with PBS and fixed in 4% formaldehyde solution. After snap

freezing in liquid nitrogen, the samples were embedded in tissue-tek O.C.T. compound (Sakura Finetechnical, Tokyo, Japan) and cut into thin sections (5 μm) for examination.

In co-localization studies, images were acquired visualizing CA (excited at 425 nm, detected at 530 nm) and Nile red (excited at 530 nm, detected 635 nm). The ZEN Image Software 2012 was used to perform the image recording and image analysis.

The image included 512 × 512 pixels measuring 2.77 × 2.77 μm². The degree of co-localization was measured by using the Image-Pro Plus 6.0, and calculated as Pearson's correlation coefficient and overlap coefficient according to Manders [33–35].

2.7. Data analysis

All data were expressed as the means ± standard deviation (SD). The pharmacokinetic parameters were calculated by non-compartmental methods by using WinNonlin software (Pharsight Corporation, Mountain View, CA, USA, Version 6.1). The SPSS statistics 17.0 was used to perform with the statistical analyses. Data were assessed by the two-tailed, unpaired Student's t-test or factorial analysis of variance (ANOVA). A P-value less than 0.05 was indicated statistically significance.

3. Results and discussion

3.1. Characterization of micelles

The hydrodynamic particle size of the CA loaded PEG–PLGA micelles was determined to be 28.01 ± 0.77 nm with a relatively narrow size distribution indicated by a polydispersity index (PDI) value of 0.112 ± 0.007 (Table 1). The zeta-potential of CA loaded micelles was −21.50 ± 0.77 mV, suggesting that the electrostatic repulsion between particles might prevent the aggregation of the vesicles and increase the stability of the dispersions. When CA was co-loaded with either Nile red or coumarin-6 at a mass ratio of 5:1, the particle size and PDI were not significantly affected, albeit the zeta-potentials decreased by approximately 10 mV (Table 1). In addition, the micelles exhibited excellent encapsulation efficiency (EE) and process robustness in the case of CA alone and also the mixtures of CA and fluorescent dyes. When the CA loading was 1.89% (w/w), the EE was higher than 98% (Table 1). The ability of PEG–PLGA micelles to encapsulate hydrophobic drugs was documented previously [32,36,37]. In the present study, the encapsulation of CA inside the micelle cores was confirmed by ¹H NMR results and the morphological examination of the micelles before and after nebulization was performed using TEM (Supplemental Figs. 1S and 2S).

The *in vitro* release profile of the micellar systems is shown in Fig. 1. It can be seen that the free CA solution led to a rapid release with more than 85% of drug released from the dialysis bag in 2 h. When encapsulated into polymeric micelles, CA was released in a sustained manner over 24 h with only ∼17.3% of initial burst within the first 2 h. In addition, the *in vitro* release study of the mixture of CA and Nile red/coumarin-6 confirmed that the
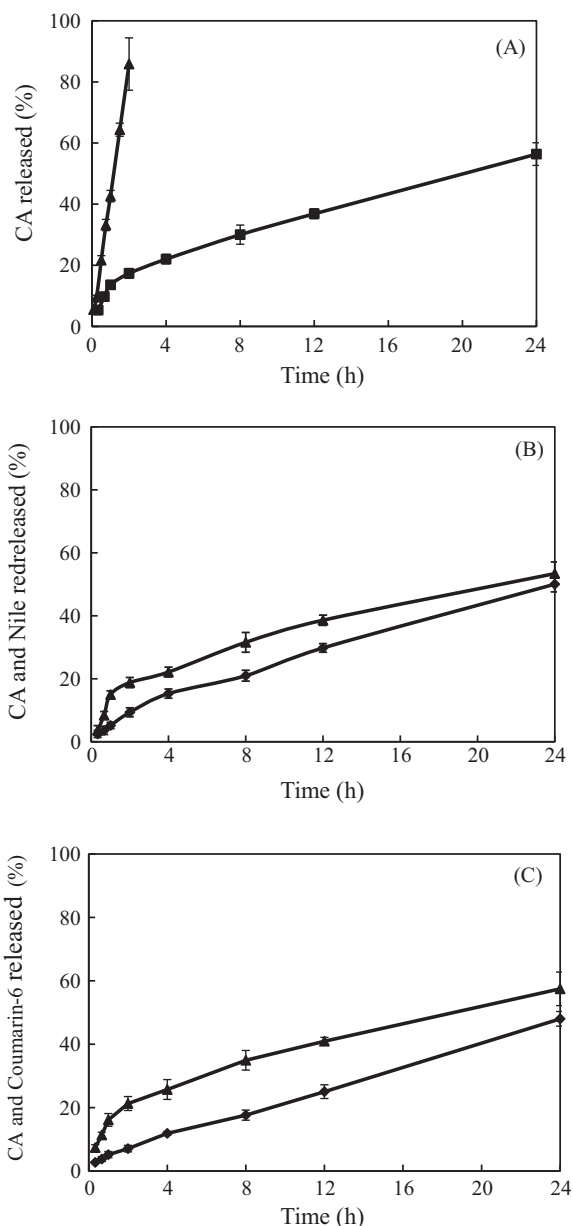

Fig. 1. *In vitro* release profiles of (A) free curcumin acetate (CA) solution (▲) and CA-loaded mPEG–PLGA micelles (♦), (B) CA (▲) and Nile red (♦) from CA and Nile red (5:1) co-loaded micelles and (C) CA (▲) and coumarin-6 (♦) from CA and coumarin-6 (5:1) co-loaded micelles (means ± SD, n = 3).

co-loaded vesicles had a similar release profile to that of CA. These *in vitro* release data suggest that PEG–PLGA micelles are potentially useful to control the release of CA and that the significantly sustained release is likely attributed to the slower diffusion of CA from the micelles rather than the penetration of drug molecules across

Table 1
Encapsulation parameters, dynamic particle size and zeta-potentials of polymeric micelles (means ± SD, n = 3).

	CA micelles	CA and Nile red micelles		CA and coumarin-6 micelles	
		CA	Nile red	CA	Coumarin-6
Drug loading (%)	1.89 ± 0.02	1.72 ± 0.01	0.36 ± 0.01	1.75 ± 0.03	0.34 ± 0.03
Encapsulation efficiency (%)	98.97 ± 0.02	98.89 ± 0.08	98.01 ± 0.03	98.22 ± 0.03	97.98 ± 0.07
Size (nm)	28.01 ± 0.77	28.72 ± 0.39		29.34 ± 0.29	
PDI	0.112 ± 0.007	0.104 ± 0.003		0.180 ± 0.008	
Zeta-potential (mV)	−21.50 ± 0.77	−11.35 ± 0.78		−9.53 ± 0.33	

the dialysis membrane. In addition, considering that the physicochemical properties and the *in vitro* release profile were not affected by co-loading with Nile red or coumarin-6, the co-encapsulated micelles might be useful for tissue localization studies.

3.2. Stability of CA in micelles

CA was instable in aqueous solution, PBS buffer (pH 7.4) medium and extremely labile in the bio-matrices (Fig. 2). As an esterified curcumin, CA was subjective to rapid chemical or esterase hydrolysis and thus converted to curcumin as indicated in HPLC chromatograms (data not shown). Incubation of CA in water or PBS buffer (pH 7.4) for 24 h resulted in approximately 75% degradation (Fig. 2A and B), whereas stability of CA when loaded into micelles, was improved to 75% intact CA. When added to rat plasma, CA was rapidly hydrolyzed to curcumin, leading to 61.2%

of degradation at 0 °C within 5 min (Fig. 2C). In contrast, the encapsulation into micelles increased the stability of CA in rat plasma in such a way that 60% degradation was observed after approximately 2 h. Therefore, the concentration ratio between CA and curcumin can be used as an indicator of the stability of CA *in vivo*, i.e., the higher the ratio, the more stable CA is. More importantly, the detection of the converted curcumin can indicate the release of CA from the micelles, enabling to determine the *in vivo* release profile of CA from the local concentration of curcumin in the lung tissue.

3.3. Pharmacokinetics

The plasma concentration–time curves of CA and converted curcumin after administration of free drug and micellar formulations are shown in Fig. 3 and the pharmacokinetic parameters are summarized in Table 2. Following IV injection of CA solution, CA rapidly was converted to curcumin and the plasma concentration decreased to below the LLOD (i.e. 8 ng/ml) within 1 h post-injection, whereas CA loaded into micelles provided extended plasma levels of CA for at least 12 h after IV administration. The IV micelles were found to increase the AUC_{CA} by 22.1-fold compared to the free drug given IV. This finding was consistent with previous data since PEGylated polymeric micelles have been well demonstrated to confer to stabilization, sustained release and consequently to enhanced plasma AUC after IV administration [32,38–40].

IT delivered CA micelles led to sustained plasma levels for up to 24 h, but when compared to CA administered by the IV route, significantly lower ($P < 0.01$) plasma levels were observed for the initial 4 h. These findings are similar to earlier result reported by
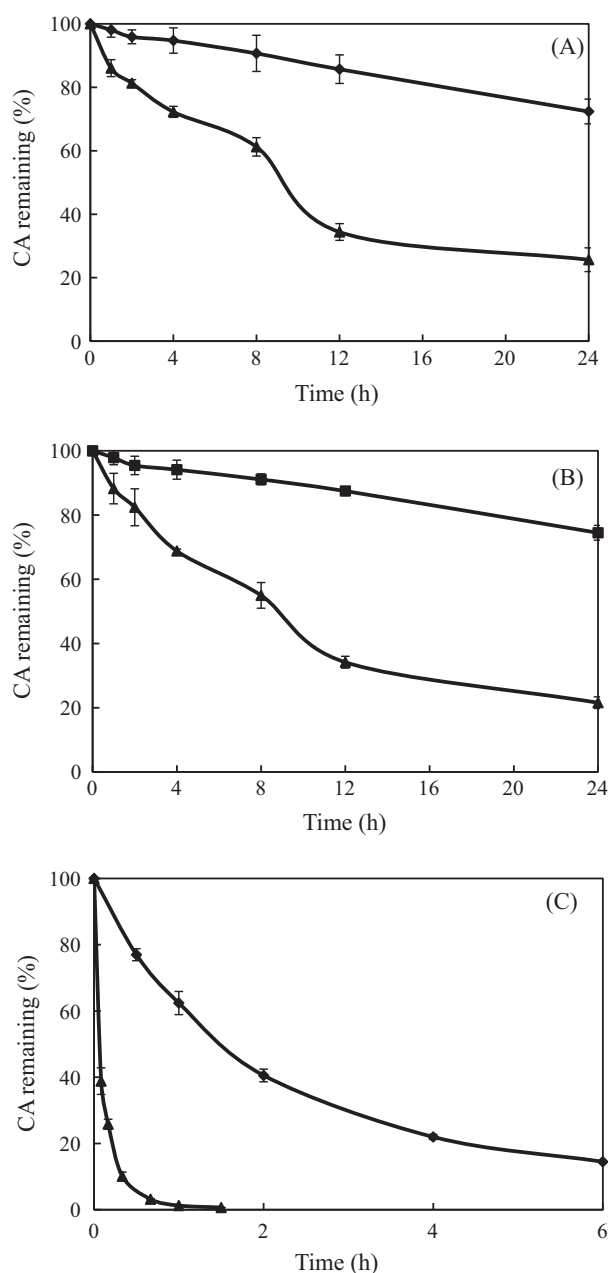

Fig. 2. Stability of curcumin acetate (CA) as free drug (▲) or loaded into micelles (♦) in (A) water, (B) PBS buffer (pH 7.4) and (C) rat plasma (means ± SD, *n* = 3).
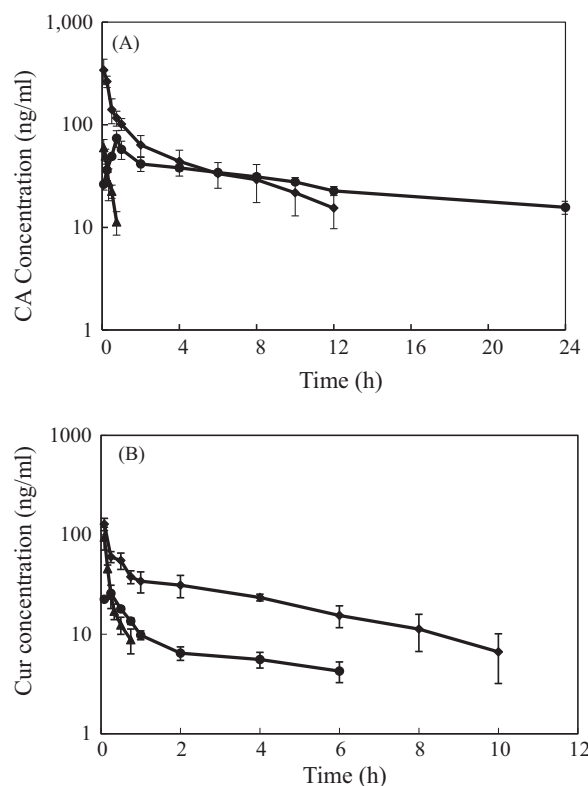

Fig. 3. Plasma concentrations of curcumin acetate (CA) (A) or curcumin (B) *versus* time after intravenous administration of free CA solution (▲) and CA loaded micelles (♦) or intratracheal administration of CA loaded micelles (●) to rats at a dose of 2 mg/kg (means ± SD, *n* = 6).

Table 2
Pharmacokinetic parameters of curcumin acetate (CA) and converted curcumin after the intravenous (IV) administration of free CA solution, and IV and intratracheal (IT) delivery of CA loaded micelles to rats at a dose of 2 mg/kg (means ± SD, $n = 6$).

Parameter	Curcumin			CA		
	Free drug (IV)	Micelles (IV)	Micelles (IT)	Free drug (IV)	Micelles (IV)	Micelles (IT)
C_0 (ng/ml)	99.0 ± 24.6	128.0 ± 18.1	–	56.5 ± 10.6	340.5 ± 94.8	–
$t_{1/2}$, λ_z (min)	15.5 ± 6.0	220.4 ± 120.8[**]	399.6 ± 53.9[**]	24.6 ± 11.8	260.8 ± 86.8[**]	931.7 ± 158.4[**]
AUC_{0-t} (μg min/ml)	1.8 ± 0.4	14.1 ± 1.3[**]	2.8 ± 0.2[*]	1.6 ± 0.2	36.5 ± 7.0[**]	39.3 ± 1.0[**]
$AUC_{0-\infty}$ (μg min/ml)	1.9 ± 0.4	16.7 ± 3.5[**]	5.3 ± 0.8[*]	2.0 ± 0.3	42.2 ± 9.4[**]	60.8 ± 7.4[**]
V_d, λ_z (l)	4.6 ± 1.0	7.3 ± 2.5	54.5 ± 13.5[**]	8.7 ± 3.0	4.2 ± 1.0	11.0 ± 0.6
CL (ml/min)	216.5 ± 40.0	24.8 ± 4.7[**]	94.5 ± 10.4[*]	254.7 ± 42.3	12.4 ± 2.9[**]	8.3 ± 0.9[**]
F (%)	–	766.4	154.4	–	2213.8	2381.0

[*] $P < 0.05$, compared to free drug.
[**] $P < 0.01$, compared to free drug.

Gill et al. who investigated paclitaxel loaded PEG$_{5000}$–DSPE micelles [30]. Plasma concentrations of converted curcumin from non-encapsulated CA could only be determined up to 1 h (>4 ng/ml), whereas IV micelles could be determined for up for to 10 h (Fig. 3B). IT micelles, on the other hand, provided sustained plasma levels of converted curcumin for 6 h, which was markedly
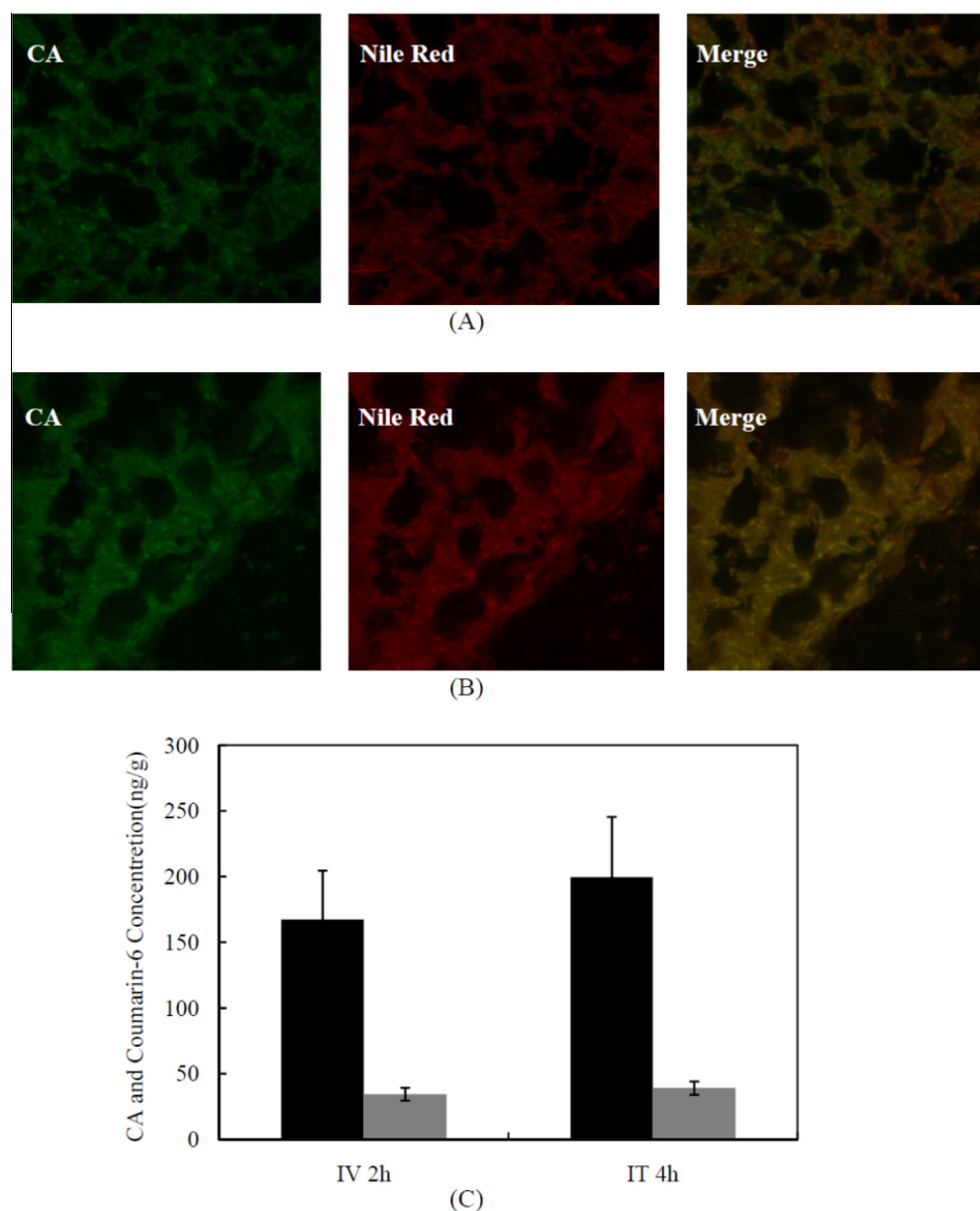

Fig. 4. Co-localization of CA with Nile red in the brain tissues suggested the distribution of micelles in the brain after intravenous (IV) (A) or intratracheal (IT) (B) administration and (C) the mean CA (■) and coumarin-6 (▨) concentration in the brain tissues at 2 h post-IV or 4 h post-IT administration. Scale bar = 10 μm.

shorter than the maximal detection time of CA. The AUC$_{Curcumin}$ for IV and IT micelles were calculated to be 7.66-fold and 1.54-fold compared to that of the free drug given IV. It should be noted that

no pharmacokinetic analysis was performed with free CA given IT due to the limited aqueous solubility of CA (i.e., <0.5 μg/ml). When AUC values of CA were compared to those of converted curcumin,

Fig. 5. Mean CA concentration–time profiles in organs after adminministration of CA solution (■), CA loaded micelles (●) and intratracheal administration of CA loaded micelles (▲) to rats at a dose of 2 mg/kg (means ± SD, *n* = 3). (A) Lung; (B) brain; (C) heart; (D) liver; (E) spleen (F) kidney and (G) axillary lymph nodes.
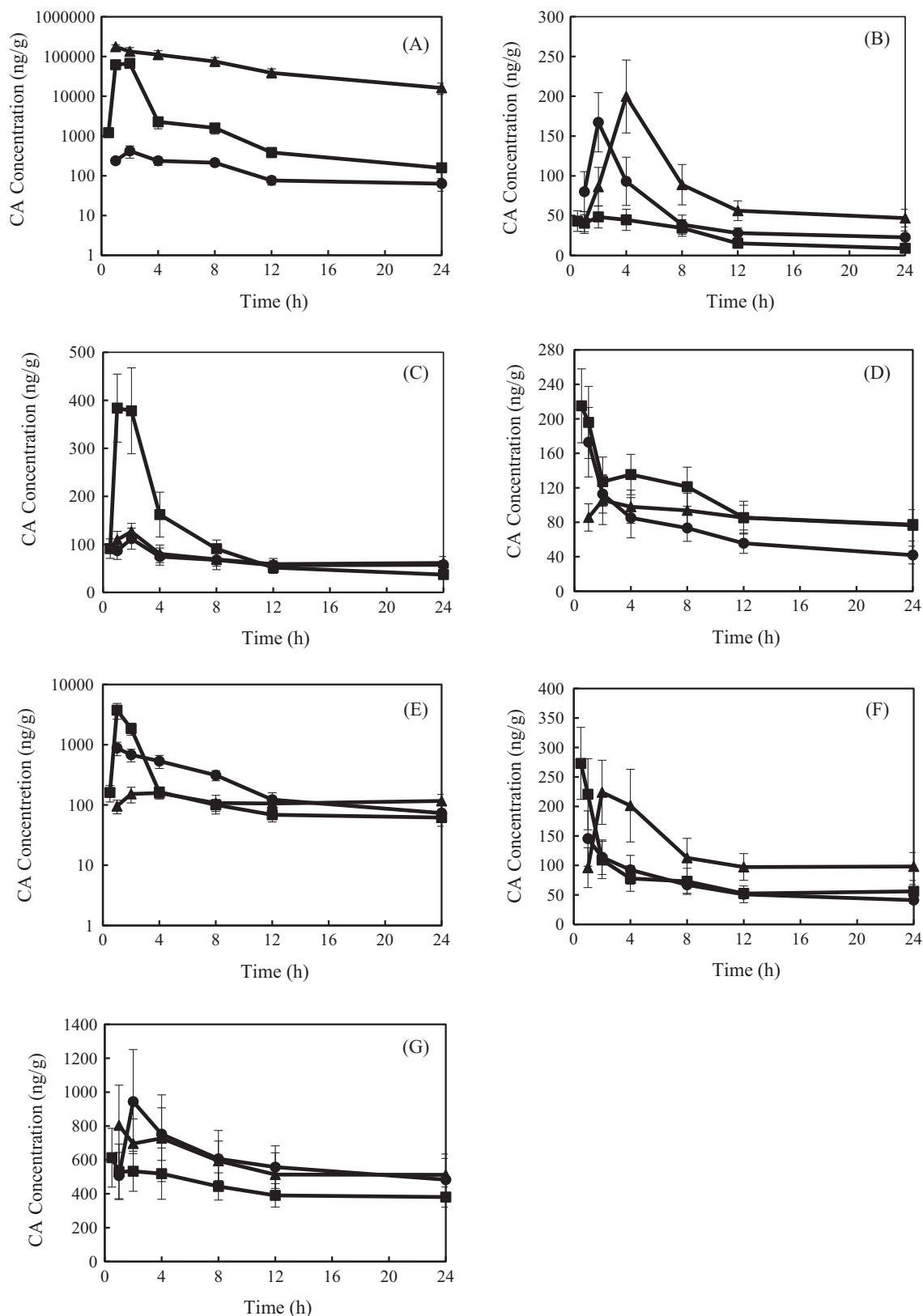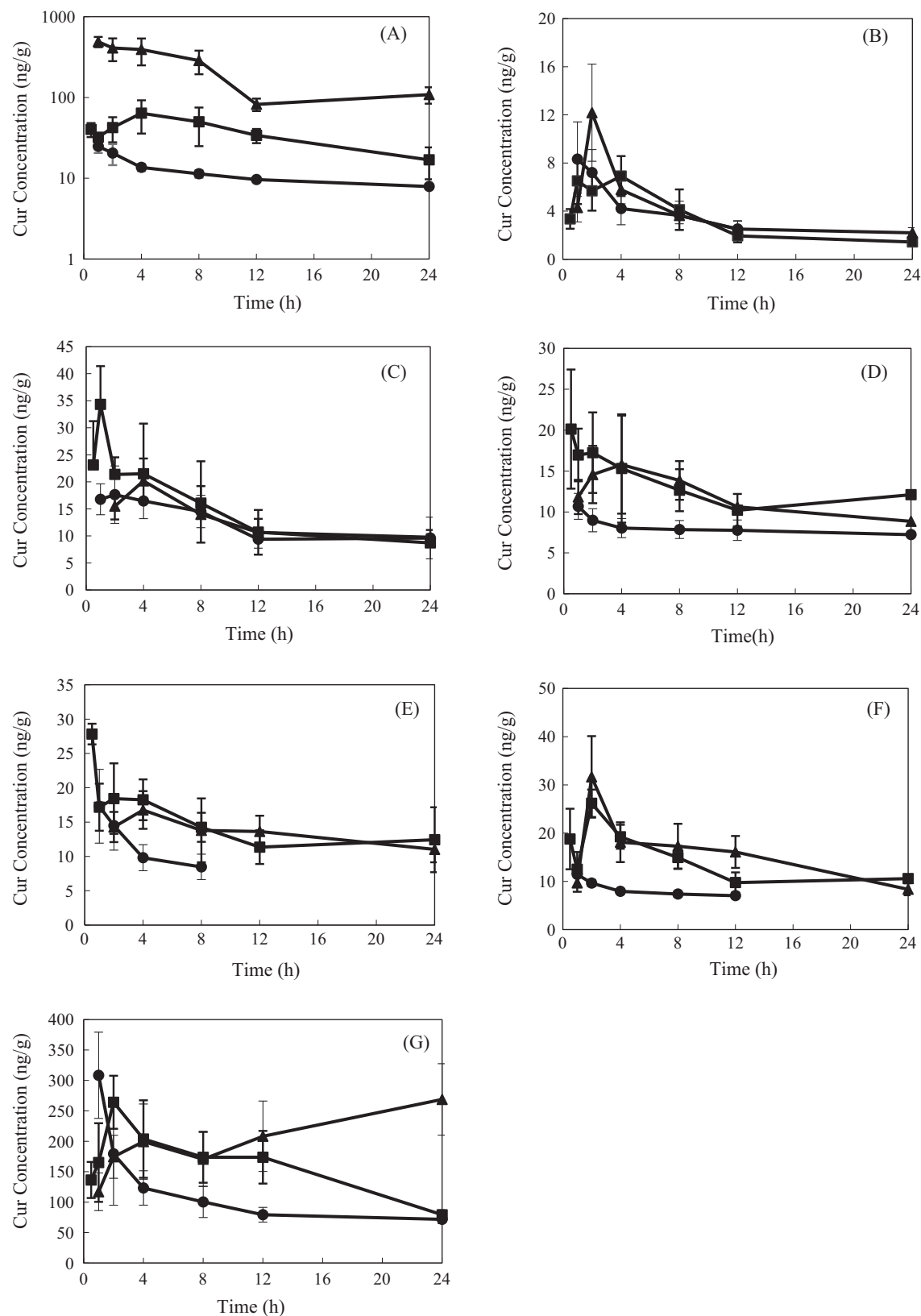
Fig. 6. Mean curcumin concentration–time profiles in organs after intravenous administration of CA solution (■), CA-loaded mPEG–PLGA micelles (●) and intratracheal administration of CA-loaded mPEG–PLGA micelles (▲) to rats with dose of 2 mg/kg (means ± SD, n = 3). (A) Lung; (B) brain; (C) heart; (D) liver; (E) spleen; (F) kidney and (G) axillary lymph nodes.

the mean ratio of AUC_{CA} to $AUC_{Curcumin}$ for free drug given IV was 0.90, which was significantly lower than the value of 2.60 calculated for IV micelles and 13.86 for IT micelles.

It is practically impossible to confirm the translocation of intact micelles from the airspace to the systemic circulation as it is tone cannot differentiate between released drug/dye and the still

encapsulated counterpart. It can be speculated that the elevated ratio of AUC_{CA} to $AUC_{Curcumin}$ in the case of IT micelles was indicative of a translocation of intact micelles across the air–blood barrier. The prolonged circulation conferred by the translocated micelles might also account for the comparable AUC_{CA} values of IT and IV administration.

To further confirm the translocation of intact micelles across the air–blood barrier, confocal microscopy was utilized to evaluate the distribution of IV and IT micelles in brain tissues. Confocal micrographs (Fig. 4A and B) of brain slices obtained after CA and Nile red co-loaded micelles were given to rats by either the IV or IT route showed a high degree of co-localization of CA and Nile red. In addition, the brain distribution of CA and coumarin-6 after IT administration of co-loaded micelles was studied, and the results confirm that the mean CA to coumarin-6 mass ratio (5.11:1) in brain tissues (Fig. 4C) was similar to the nominal loading ratio (5.14:1) in the micelles (Table 1). Considering that coumarin-6 is practically impermeable to the blood–brain barrier (BBB) [41], it could be deduced that coumarin-6 penetrated through the BBB encapsulated into micelles. In the literature, little is known about the translocation of the inhaled pharmaceutical nanocarriers from a biopharmaceutical point of view [42]. Existing data on the translocation of nanomaterials across the air–blood barrier mainly come from the epidemiologic and toxicological studies of inhaled environmental nanoparticles and the majority of these studies suggest that only a minor fraction of inhaled nanoparticles, including PEGylated metal nanoparticles, may actually permeate into the systemic circulation and accumulate in extra-pulmonary organs [43–46]. However, our current study has demonstrated that IT micelles could efficiently penetrate the air–blood barrier. The significant extent by which our polymeric micelles entered the blood circulation and extra-pulmonary organs can be appreciated by the AUC_{CA} values in plasma and brain tissue, which were comparable to those of the IV dose.

3.4. Tissue distribution

The tissue distribution data of CA and the converted curcumin for free drug and micellar formulations after IV or IT administration are shown in Figs. 5 and 6, and the $AUC_{0–24\ h}$ values are listed in Table 3. The results show that free CA given IV resulted in higher lung distribution relative to the IV micelles, possibly due to the high lipophilicity of the drug. The IT micelles, however, always led to significantly higher lung concentrations of CA than IV administration, with the AUC values of pulmonary CA being 8.6- and 400-fold higher than those of IV free drug and micelles, respectively. To further evaluate the localization of micelles in the lung, confocal microscopy of lung slices after IV and IT administration was performed (Fig. 7). The results show that both CA and Nile red with high co-localization degree were distributed in pulmonary arterial endothelial tissue, suggesting the uptake of micelles into

vascular endothelial cells. In addition, IT micelles showed higher and more sustained local concentrations of CA in pulmonary arterial endothelia in terms of fluorescent intensity, relative to IV micelles. Indeed, the fluorescence activity observed in lung slices 24 h post-IV injection was rather dim compared to that in corresponding IT lung samples. In good agreement with tissue distribution data from Fig. 5A, the imaging results also suggest that IT micelles conferred to the higher accumulation of CA to in the pulmonary vascular endothelium relative to IV given micelles.

In terms of the lung concentrations of converted curcumin, which represents the drug released from the micelles and thus the true amount of locally available drug, IT micelles also brought about markedly higher AUC in the lung, with approximately 5.4- and 16.9-fold increases when compared to intravenously administered free drug and micelles, respectively. According to a recent study, curcumin (at a daily oral dose of 100 mg/kg) was found to significantly decrease pulmonary arterial pressure, the ratio of right ventricle to body weight and the wall thickening and stenosis of pulmonary blood vessel, in MCT induced PAH rats [3]. At this dose, the curcumin concentration in the lung was about 200 ng/g [29]. The high sustained curcumin lung concentrations achieved by the CA loaded micelles after IT administration might make them interesting new tools for PAH treatment. Nonetheless, it should be noted that IT administration in the present study was used as a means to deliver the formulation to rats with a view to facilitating accurate dosing to experimental animals. As for the intended clinical application, a dry powder inhaler (DPI) of spray-dried particles or a nebulized solution reconstituted from freeze-dried powders, rather than IT instillation, would be the options for the pulmonary delivery of micelles.

The targeting efficiency (Te) to the lung, which was calculated using the following equation, was considered as an important parameter for assessing targeted delivery [30].

$$Te = \frac{AUC_{0-24h}\ (\text{target tissue})}{\sum_{i=0} AUC_{0-24h}\ (\text{non-target tissue})}$$

The Te of CA to the lung from IT micelles was 55.8, which was 6.02- and 436-fold higher than that of free drug and micelle given IV, respectively, whereas the Te (lung) of converted curcumin from IT micelles was 0.75, which was 2.86- and 10.1-fold higher than what was calculated for IV free drug and micelles, respectively. In the literature, the total drug content recovered in the lung was used to indicate lung availability due to the inability to differentiate between released drug and drug within a carrier [47]. The dramatic difference in Te between CA and converted curcumin observed in our study suggested that caution should be taken when the encapsulated drug content is included in the calculation of locally available drug. Understanding the in vivo release profile may be essential to determine the true local availability of inhaled sustained release carriers. As for the distribution patterns in other tissues, the differences in AUC of CA and curcumin in the liver,

Table 3
AUC values of curcumin acetate (CA) and converted curcumin in tissues and targeting efficiency (Te) to lungs in three groups of rats ($n = 3$) after intravenous (IV) administration of free CA and CA-loaded micelles and intratracheal (IT) administration of CA loaded micelles at a dose of 2 mg/kg.

Tissues	Curcumin AUC_{0-24h} (µg h/ml)			CA AUC_{0-24h} (µg h/ml)		
	Free drug (IV)	Micelles (IV)	Micelles (IT)	Free drug (IV)	Micelles (IV)	Micelles (IT)
Heart	0.34	0.29	0.30	2.41	1.59	1.66
Liver	0.31	0.19	0.27	2.54	1.72	2.05
Spleen	0.34	0.12	0.31	7.53	6.74	2.77
Lung	0.88	0.28	4.74	165	3.54	1420
Kidney	0.32	0.18	0.36	1.83	1.61	2.85
Brain	0.077	0.081	0.08	0.58	1.17	1.86
Axillary lymph nodes	1.93	2.68	4.94	2.92	14.23	13.6
Plasma	0.030	0.23	0.047	0.027	0.61	0.65
Te to lung	0.26	0.07	0.75	9.27	0.13	55.8

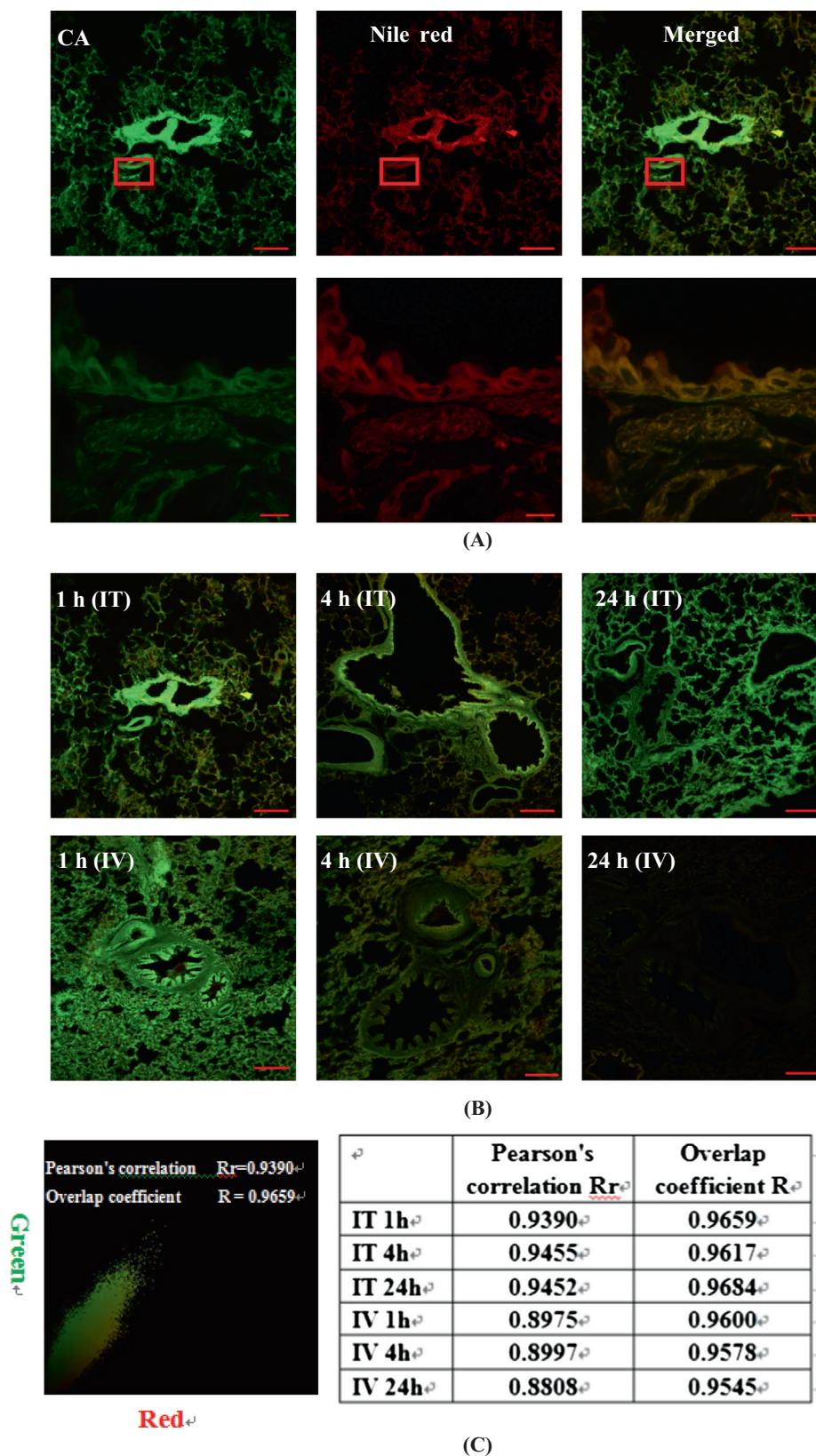|	Pearson's correlation Rr	Overlap coefficient R
IT 1h	0.9390	0.9659
IT 4h	0.9455	0.9617
IT 24h	0.9452	0.9684
IV 1h	0.8975	0.9600
IV 4h	0.8997	0.9578
IV 24h	0.8808	0.9545

Fig. 7. (A) Co-localization of CA with Nile red in lung tissues in pulmonary arteries at 1 h after IT administration, scale bar = 200 μm (top), scale bar = 10 μm (bottom). (B) Co-localization of CA with Nile red in lung tissues after IT and IV administration, scale bar = 200 μm. (C) The Pearson's correlation coefficient (PCC) and overlap coefficient according to Manders (MOC) in pulmonary arteries after IT and IV administration.

kidney, heart, brain, spleen and axillary lymph nodes appeared to be marginal to moderate (<3-fold) distinct from the pronounced difference (400-fold) in the AUC of CA in the lung, when comparing IT micelles with IV ones. This result suggests that IT micelles can achieve high Te in the lung but did not markedly increase accumulation in non-targeted tissues, potentially leading to an extended therapeutic window.

Another important finding in this study was that IT micelles resulted in enhanced or comparable AUC values of CA in the brain and lymph nodes, when compared to the IV counterparts. The increased distribution to the brain and lymph nodes might be attributed to the ability of micelles to penetrate across the BBB [48] and to accumulate in the lymphatic system via extravasation [49]. The fact that IT micelles can translocate across the air–blood barrier to the blood and penetrate into the brain suggests that pulmonary delivery may be able to non-invasively achieve brain targeting with nanocarriers.

Both the hydrophilic block, PEG, and the hydrophobic block, PLGA of the PEG–PLGA block co-polymer are most often used for drug delivery systems and have been approved by Food and Drug Administration for therapeutic injections. The pulmonary compatibility was also demonstrated in previous studies *in vitro* and *in vivo* [50]. In the present study, PEG–PLGA micelles only exhibited marginal inhibitory effect on Calu-3 cell viability up to a concentration of 5 mg/ml after 24 h exposure (Supplemental Fig. S3). In addition, following IT administration to rats, both blank and CA loaded micelles exhibited comparable biocompatibility to saline in terms of the LDH activity in bronchialalveolar lavage fluids (Supplemental Fig. S4). As a result, the present results suggested that the micelle was well biocompatible to the lung.

4. Conclusions

The present study examined the *in vitro* release profile and *in vivo* pharmacokinetics and translocation properties of mPEG–PLGA micelles intended for pulmonary drug administration. The *in vivo* results demonstrated that micelles administered by the pulmonary route not only prolonged the pulmonary retention time and facilitated the uptake to the pulmonary vascular endothelium, but also achieved local sustained release, suggesting that inhalable micelles might represent interesting carriers for the local delivery of anti-PAH drugs. In addition, aerosolized micelles appeared to efficiently translocate across the air–blood barrier into the bloodstream and distribute to extra-pulmonary organs including the brain as intact micellar vesicles in a sustained release manner, indicating the potential for non-invasive systemic sustained release.

Appendix A. Supplementary material

Supplementary data associated with this article can be found, in the online version, at http://dx.doi.org/10.1016/j.ejpb.2014.10.010.

References

[1] A. Shehzad, G. Rehman, Y.S. Lee, Curcumin in inflammatory diseases, BioFactors 39 (2013) 69–77.

[2] Q. Lin, L.X. Wang, S.X. Chen, X.F. Zhou, X.Y. Huang, X.F. Fan, Effect of curcumin on pulmonary hypertension and wall collagen of pulmonary arterioles of chronic hypoxic hypercapnic rats, Chin. J. Appl. Physiol. 22 (2006) 257–261.

[3] H. Liao, Research of the Effect of Curcumin on Pulmonary Hypertension and its Mechanism, Master's Degree Thesis of Fudan University, 2011.

[4] E. Bronte, G. Coppola, R. Di Miceli, V. Sucato, A. Russo, S. Novo, Role of curcumin in idiopathic pulmonary arterial hypertension treatment: a new therapeutic possibility, Med. Hypotheses 81 (2013) 923–926.

[5] L.R. Frumkin, The pharmacological treatment of pulmonary arterial hypertension, Pharmacol. Rev. 64 (2012) 583–620.

[6] L.J. Rubin, D.B. Badesch, R.J. Barst, N. Galie, C.M. Black, A. Keogh, T. Pulido, A. Frost, S. Roux, I. Leconte, M. Landzberg, G. Simonneau, Bosentan therapy for pulmonary arterial hypertension, N. Engl. J. Med. 346 (2002) 896–903.

[7] R. Ewert, C.F. Opitz, R. Wensel, J. Winkler, M. Halank, S.B. Felix, Continuous intravenous iloprost to revert treatment failure of first-line inhaled iloprost therapy in patients with idiopathic pulmonary arterial hypertension, Clin. Res. Cardiol. 96 (2007) 211–217.

[8] P.A. Corris, Alternatives to lung transplantation: treatment of pulmonary arterial hypertension, Clin. Chest Med. 32 (2011) 399–410.

[9] V.V. McLaughlin, H.I. Palevsky, Parenteral and inhaled prostanoid therapy in the treatment of pulmonary arterial hypertension, Clin. Chest Med. 34 (2013) 825–840.

[10] B.L. LeVarge, R.N. Channick, Inhaled treprostinil for the treatment of pulmonary arterial hypertension, Exp. Rev. Respir. Med. 6 (2012) 255–265.

[11] F. Ichinose, J. Erana-Garcia, J. Hromi, Y. Raveh, R. Jones, L. Krim, M.W.H. Clark, J.D. Winkler, K.D. Bloch, W.M. Zapol, Nebulized sildenafil is a selective pulmonary vasodilator in lambs with acute pulmonary hypertension, Crit. Care Med. 29 (2001) 1000–1005.

[12] T. Gessler, W. Seeger, T. Schmehl, Inhaled prostanoids in the therapy of pulmonary hypertension, J. Aerosol Med. 21 (2008) 1–12.

[13] H. Olschewski, G. Simonneau, N. Galie, T. Higenbottam, R. Naeije, L.J. Rubin, S. Nikkho, R. Speich, M.M. Hoeper, J. Behr, J. Winkler, O. Sitbon, W. Popov, H.A. Ghofrani, A. Manes, D.G. Kiely, R. Ewert, A. Meyer, P.A. Corris, M. Delcroix, M. Gomez-Sanchez, H. Siedentop, W. Seeger, Inhaled iloprost for severe pulmonary hypertension, N. Engl. J. Med. 347 (2002) 322–329.

[14] V. Gupta, A. Rawat, F. Ahsan, Feasibility study of aerosolized prostaglandin E1 microspheres as a noninvasive therapy for pulmonary arterial hypertension, J. Pharm. Sci. 99 (2010) 1774–1789.

[15] V. Gupta, M. Davis, L.J. Hope-Weeks, F. Ahsan, PLGA microparticles encapsulating prostaglandin E1-hydroxypropyl-β-cyclodextrin (PGE1-HPβCD) complex for the treatment of pulmonary arterial hypertension (PAH), Pharm. Res. 28 (2011) 1733–1749.

[16] V. Gupta, N. Gupta, I.H. Shaik, R. Mehvar, E. Nozik-Grayck, I.F. McMurtry, M. Oka, M. Komatsu, F. Ahsan, Inhaled PLGA particles of prostaglandin E1 ameliorate symptoms and progression of pulmonary hypertension at a reduced dosing frequency, Mol. Pharm. 10 (2013) 1655–1667.

[17] A. Saigal, W.K. Ng, R.B. Tan, S.Y. Chan, Development of controlled release inhalable polymeric microspheres for treatment of pulmonary hypertension, Int. J. Pharm. 450 (2013) 114–122.

[18] B. Stark, F. Andreae, P. Debbage, W. Mosgoeller, R. Prassl, Association of vasoactive intestinal peptide with polymer-grafted liposomes: structural aspects for pulmonary delivery, Biochim. Biophys. Acta 1768 (2007) 705–714.

[19] E. Kleemann, T. Schmehl, T. Gessler, U. Bakowsky, T. Kissel, W. Seeger, Iloprost-containing liposomes for aerosol application in pulmonary arterial hypertension: formulation aspects and stability, Pharm. Res. 24 (2007) 277–287.

[20] V. Gupta, N. Gupta, I.H. Shaik, R. Mehvar, I.F. McMurtry, M. Oka, E. Nozik-Grayck, M. Komatsu, F. Ahsan, Liposomal fasudil, a rho-kinase inhibitor, for prolonged pulmonary preferential vasodilation in pulmonary arterial hypertension, J. Control. Release 167 (2013) 189–199.

[21] S. Kimura, K. Egashira, L. Chen, K. Nakano, E. Iwata, M. Miyagawa, H. Tsujimoto, K. Hara, R. Morishita, K. Sueishi, R. Tominaga, K. Sunagawa, Nanoparticle-mediated delivery of nuclear factor kappa B decoy into lungs ameliorates monocrotaline-induced pulmonary arterial hypertension, Hypertension 53 (2009) 877–883.

[22] L. Chen, K. Nakano, S. Kimura, T. Matoba, E. Iwata, M. Miyagawa, H. Tsujimoto, K. Nagaoka, J. Kishimoto, K. Sunagawa, K. Egashira, Nanoparticle-mediated delivery of pitavastatin into lungs ameliorates the development and induces regression of monocrotaline-induced pulmonary artery hypertension, Hypertension 57 (2011) 343–350.

[23] M. Harada-Shiba, I. Takamisawa, K. Miyata, T. Ishii, N. Nishiyama, K. Itaka, K. Kangawa, F. Yoshihara, Y. Asada, K. Hatakeyama, N. Nagaya, K. Kataoka, Intratracheal gene transfer of adrenomedullin using polyplex nanomicelles attenuates monocrotaline-induced pulmonary hypertension in rats, Mol. Ther. 17 (2009) 1180–1186.

[24] C. Plumley, E.M. Gorman, N. El-Gendy, C.R. Bybee, E.J. Munson, C. Berkland, Nifedipine nanoparticle agglomeration as a dry powder aerosol formulation strategy, Int. J. Pharm. 369 (2009) 136–143.

[25] M. Beck-Broichsitter, A.C. Dalla-Bona, T. Kissel, W. Seeger, T. Schmehl, Polymer nanoparticle-based controlled pulmonary drug delivery, Methods Mol. Biol. 1141 (2014) 133–145.

[26] J.U. Menon, P. Ravikumar, A. Pise, D. Gyawali, C.C. Hsia, K.T. Nguyen, Polymeric nanoparticles for pulmonary protein and DNA delivery, Acta Biomater. 10 (2014) 2643–2652.

[27] J. Varshosaz, S. Taymouri, H. Hamishehkar, Fabrication of polymeric nanoparticles of poly (ethylene-co-vinyl acetate) coated with chitosan for

pulmonary delivery of carvedilol, J. Appl. Polym. Sci. 131 (2014), http://dx.doi.org/10.1002/app.39694.

[28] R. Parikh, S. Dalwadi, Preparation and characterization of controlled release poly-ε-caprolactone microparticles of isoniazid for drug delivery through pulmonary route, Powder Technol. 264 (2014) 158–165.

[29] V.R. Devadasu, R.M. Wadsworth, M.N. Ravi Kumar, Tissue localization of nanoparticles is altered due to hypoxia resulting in poor efficacy of curcumin nanoparticles in pulmonary hypertension, Eur. J. Pharm. Biopharm. 80 (2012) 578–584.

[30] K.K. Gill, S. Nazzal, A. Kaddoumi, Paclitaxel loaded PEG_{5000}–DSPE micelles as pulmonary delivery platform: formulation characterization, tissue distribution, plasma pharmacokinetics, and toxicological evaluation, Eur. J. Pharm. Biopharm. 79 (2011) 276–284.

[31] S. Edsbäcker, C.J. Johansson, Airway selectivity: an update of pharmacokinetic factors affecting local and systemic disposition of inhaled steroids, Basic Clin. Pharmacol. Toxicol. 98 (2006) 523–536.

[32] X. Hu, R. Han, L.H. Quan, C.Y. Liu, Y.H. Liao, Stabilization and sustained release of zeylenone, a soft cytotoxic drug, within polymeric micelles for local antitumor drug delivery, Int. J. Pharm. 450 (2013) 331–337.

[33] S. Schneider, D. Lenz, M. Holzer, K. Palme, R. Süss, Intracellular FRET analysis of lipid/DNA complexes using flow cytometry and fluorescence imaging techniques, J. Control. Release 145 (2010) 289–296.

[34] S. Bolte, F.P. Cordelieres, A guided tour into subcellular colocalization analysis in light microscopy, J. Microsc. 224 (2006) 213–232.

[35] V. Zinchuk, O. Zinchuk, T. Okada, Quantitative colocalization analysis of multicolor confocal immunofluorescence microscopy images: pushing pixels to explore biological phenomena, Acta Histochem. Cytochem. 40 (2007) 101–111.

[36] S.W. Choi, J.H. Kim, Design of surface-modified poly(D,L-lactide-co-glycolide) nanoparticles for targeted drug delivery to bone, J. Control. Release 122 (2007) 24–30.

[37] D.G. Yao, K.X. Sun, H.J. Mu, F.M. Zhou, H.H. Chen, L.J. Liu, N. Liang, Preparation of cyclosporine A loaded mPEG–PLGA copolymer micelles and study its pharmacokinetics in rats, Yao Xue Xue Bao 44 (2009) 1410–1415.

[38] S.C. Kim, D.W. Kim, Y.H. Shim, J.S. Bang, H.S. Oh, S.W. Kim, M.H. Seo, In vivo evaluation of polymeric micellar paclitaxel formulation: toxicity and efficacy, J. Control. Release 72 (2001) 192–202.

[39] O. Molavi, Z. Ma, A. Mahmud, A. Alshamsan, J. Samuel, R. Lai, G.S. Kwon, A. Lavasanifar, Polymeric micelles for the solubilization and delivery of STAT3 inhibitor cucurbitacins in solid tumors, Int. J. Pharm. 347 (2008) 118–127.

[40] H.C. Shin, A.W. Alani, D.A. Rao, N.C. Rockich, G.S. Kwon, Multi-drug loaded polymeric micelles for simultaneous delivery of poorly soluble anticancer drugs, J. Control. Release 140 (2009) 294–300.

[41] S.S. Bhattacharyyaa, S. Paula, A. Dea, D. Dasa, A. Samaddera, N. Boujedainib, A.R. Khuda-Bukhsh, Poly (lactide-co-glycolide) acid nanoencapsulation of a synthetic coumarin: cytotoxicity and bio-distribution in mice, in cancer cell line and interaction with calf thymus DNA as target, Toxicol. Appl. Pharmacol. 253 (2011) 270–281.

[42] J.S. Patton, J.D. Brain, L.A. Davies, J. Fiegel, M. Gumbleton, K.J. Kim, M. Sakagami, R. Vanbever, C. Ehrhardt, The particle has landed – discerning the fate of inhaled pharmaceuticals, J. Aerosol Med. Pulm. Drug Deliv. 23 (2010) S71–87.

[43] M. Geiser, W.G. Kreyling, Deposition and biokinetics of inhaled nanoparticles, Part. Fibre Toxicol. 7 (2010) 2.

[44] H.S. Choi, Y. Ashitate, J.H. Lee, S.H. Kim, A. Matsui, N. Insin, M.G. Bawendi, M. Semmler-Behnke, J.V. Frangioni, A. Tsuda, Rapid translocation of nanoparticles from the lung airspaces to the body, Nat. Biotechnol. 28 (2010) 1300–1303.

[45] J. Lipka, M. Semmler-Behnke, R.A. Sperling, A. Wenk, S. Takenaka, C. Schleh, T. Kissel, W.J. Parak, W.G. Kreyling, Biodistribution of PEG-modified gold nanoparticles following intratracheal instillation and intravenous injection, Biomaterials 31 (2010) 6574–6581.

[46] J. Zhang, L. Wu, H.K. Chan, W. Watanabe, Formation, characterization, and fate of inhaled drug nanoparticles, Adv. Drug Deliv. Rev. 63 (2011) 441–455.

[47] R.K. Verma, J. Kaur, K. Kumar, A.B. Yadav, A. Misra, Intracellular time course, pharmacokinetics, and biodistribution of isoniazid and rifabutin following pulmonary delivery of inhalable microparticles to mice, Antimicrob. Agents Chemother. 52 (2008) 3195–3201.

[48] E. Garcia-Garcia, K. Andrieux, S. Gil, P. Couvreur, Colloidal carriers and blood–brain barrier (BBB) translocation: a way to deliver drugs to the brain?, Int J. Pharm. 298 (2005) 274–292.

[49] L. Qin, F. Zhang, X. Lu, X. Wei, J. Wang, X. Fang, D. Si, Y. Wang, C. Zhang, R. Yang, C. Liu, W. Liang, Polymeric micelles for enhanced lymphatic drug delivery to treat metastatic tumors, J. Control. Release 171 (2013) 133–142.

[50] B. Patel, V. Gupta, F. Ahsan, PEG–PLGA based large porous particles for pulmonary delivery of a highly soluble drug, low molecular weight heparin, J. Control. Release 162 (2012) 310–320.